#24-027
2024 AFS Proceedings ©American Foundry Society

Evaluation of Thermal Technologies for Thermal Management of Permanent Molds

Cheolmin Ahn, Carl Söderhjelm, Diran Apelian
Advanced Casting Research Center (ACRC), University of California, Irvine, California, USA

Copyright 2024 American Foundry Society

ABSTRACT
Thermal management can play a pivotal role in the production of high-quality castings and the reduction of production cycle time by ensuring desired solidification patterns during dynamic casting processes such as permanent mold and diecasting processes. These processes require rapid heat removal and careful heat recovery for subsequent casting cycles, unlike traditional batch processes. Moreover, thermal management in specific localized regions of the mold is needed due to diverse mold geometries and shapes, as well as recent applications such as gigacasting. Local control of heat transfer for thermal management can be accomplished with the application of various thermal technologies, both heating and cooling. In this work, heat transfer characteristics of various thermal technologies were evaluated quantitatively through both modeling and experimental work.

Keywords: thermal management, thermal technologies heat transfer coefficient, heat flux, kinetics of heat flow

INTRODUCTION

Thermal management plays a pivotal role in the production of high-quality castings and the reduction of cycle time. In addition, thermal management can also increase mold life and decrease thermal fatigue, and thus manufacturing costs.[1] In contrast, inability to manage the thermal conditions cycle after cycle, will contribute to quality characteristics such as porosity, shrinkage, etc.

In general, metallic chills have been widely used to control localized cooling rates in specific designated areas in disposable molds, such as sand castings.[2] However, in dynamic casting processes like permanent mold casting and diecasting, the processes need to not only rapidly dissipate the heat but also recover the heat for subsequent casting cycles. For efficient heat dissipation, coolants are employed through cooling channels to remove the heat rapidly and enable the rapid solidification of the molten metal.

Heat transfer capabilities of coolants have been studied previously with variations of operating parameters.[3-6] However, rapid cooling rates may result in premature solidification of the molten metal from the gate system during the filling stage. It will cause incomplete cavity filling and the formation of a pre-solidified frozen front layer at the cavity surface. This issue is particularly exacerbated in thin-walled castings. The challenge is that the mold should be hot enough for the filling of the molten metal to occur without premature solidification, and yet the mold should remove heat as rapidly as possible to reduce cycle time and to ensure complete solidification.

To efficiently regulate the local temperature of the mold, many heating technologies have been suggested to increase mold temperatures[7] for proper filling of the die cavity. However, the elevated mold temperature will, conversely, require longer solidification times which will increase process cycle time and decrease productivity. Moreover, controlling the thermal profile locally and in a dynamic environment cycle after cycle is difficult.

Although previous research has yielded a certain level of understanding regarding the heat transfer characteristics of various thermal technologies,[8-17] the available knowledge is both limited and fragmented to be applied to permanent mold casting systems. The primary objective of this study is to comprehensively evaluate the heat transfer characteristics of various thermal technologies both experimentally and through simulation and modeling. Heat transfer behaviors of various technologies are explored by evaluating for each technology (i) the maximum temperature that can be attained by the steel die, (ii) the heat flux, (iii) convective and interfacial heat transfer coefficients, and (iv) the kinetics of heating/cooling technologies. These results will serve as a foundation for the development of guidelines for the selection of efficient thermal technologies based on specific casting conditions.

HEAT TRANSFER DURING SOLIDIFICATION – THEORETICAL FRAMEWORK

Heat dissipation rate during solidification is controlled by a variety of thermal resistances such as conduction, convection, and radiation.[2] The thermal resistance influences temperature distribution during the casting, as depicted in Fig. 1.

Interface between the mold and metal

For permanent molds, the heat transfer process is predominantly governed by the thermal resistance at the metallic mold interface. Specifically, a notable temperature drop occurs at the interface between the

solidified metal and the mold due to the presence of a thermal resistance at the interface, as shown in Fig. 1.

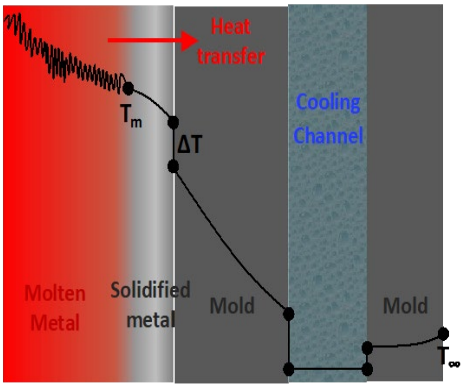

Figure 1. Temperature profile across a permanent mold casting system with the effect of thermal resistances. (T_m = melting temperature of the metal, ΔT= temperature difference between the solidified metal and the mold, and T_∞= ambient temperature)

In this regard, the solidification thickness can be expressed as a function of several variables, namely, temperature gradient, time, density, heat of fusion, and thermal resistance, which is characterized by the interfacial heat transfer coefficient (IHTC), as shown in Eqn.1.[18]

$$S = h \cdot \frac{(T_m - T_o)}{\rho_s \cdot H} \cdot t \qquad \text{Eqn.1}$$

Where: S = solidification thickness; h = interfacial heat transfer coefficient (IHTC); T_m and T_o = liquid molten metal temperature and ambient temperature, respectively; ρ_s = density of a solid; H = heat of fusion; and t = total solidification time. In practice and during commercial production conditions, this scenario is accentuated by the formation of an air gap due to volume change that occurs during solidification (5-8%).[19] In addition to the formation of the air gap, the roughness of the mold surface and the wear of the coating on the surface significantly contribute to the increase of thermal resistances at the interface. Generally, a thermal coating is applied to the permanent mold to prevent premature freezing and die soldering. The coatings usually contain graphite, clay, and sodium silicate, with thermal conductivities ranging between 0.1 to 0.3W/m·K.[20] Consequently, the thermal resistance at the interface can be influenced by several factors, such as the type and thickness of the coating and the surface roughness created by the coating. Furthermore, several other factors, including the flow rate of the liquid molten metal, die soldering, mold geometry, and pressure, may also influence the thermal resistance at the interface.[21,22]

Importance of heat transfer coefficients

Although the presence of thermal resistances has been identified, managing these resistances during the permanent mold casting process is a challenge. Understanding heat transfer coefficients is essential for efficient casting simulation and mold temperature prediction. These coefficients depend on mold surface area, geometry, and temperature function. In addition, they can be employed to generalize for various mold geometries.

Theoretically, the heat transfer coefficient is inversely related to thermal resistance. As explained next, it is classified into the convective heat transfer coefficient (h) and the interfacial heat transfer coefficient (IHTC). The heat transfer coefficients characterize the effectiveness of the heat transfer process and help to optimize thermal applications, including heating and cooling systems for thermal management of the mold.

Convective heat transfer coefficient (h)

The convective heat transfer coefficient (h) represents the heat transfer rate between a mold surface and the surrounding fluid (gas or liquid) through convection, such as direct flame, hot oil, hot water, and coolants. The h value is calculated using Newton's law of cooling (Eqn. 2).[23]

$$h_{convective} = q \,/\, (T_\infty - T_s) \qquad \text{Eqn.2}$$

Where: $h_{convective}$ = convective heat transfer coefficient (W/m^2·°C), q = heat flux (W/m^2), T_∞ and T_s = ambient temperature and surface temperature of the mold (°C), respectively.

Interfacial heat transfer coefficient (IHTC)

The interfacial heat transfer coefficient (IHTC) represents the heat transfer rate between two adjacent materials through direct conduction. Understanding how efficiently heat can pass from one material to another is crucial. In casting applications, IHTC is highly relevant at the interface between the solidified metal and the mold, as depicted in Fig. 1. Additionally, it is critical for the interface between a heating cartridge and the mold for resistant heating. The IHTC value is quantitatively determined using experimental data, as outlined in Eqn. 3.[24]

$$h_{interfacial} = q/(T_1 - T_2) \qquad \text{Eqn.3}$$

Where: $h_{interfacial}$ refers to the interfacial heat transfer coefficient (W/m^2·°C), q is a heat flux from the high-temperature area to the low-temperature area, and T_1 and T_2 are the temperatures of the heat source and the steel (°C), respectively.

Heat flux

The heat flux (q) represents the rate of heat energy transfer through a given surface per unit area and is calculated using Eqn. 4. In other words, it quantifies how

much heat is transferred through or across a surface within a specific period.

$$q = \left(\rho \cdot C_p \cdot V \cdot \left(\frac{\partial T}{\partial t}\right)\right) \div A \qquad \text{Eqn.4}$$

Where: ρ = density of the steel die (kg/m^3), C_p = the specific heat (J/kg·°C), V = volume of the steel die (m^3), and A = surface area of the steel die (m^2).

In this study, the heat flux of the steel die is calculated with average temperatures of the steel as a function of time during heating and cooling experiments.

Table 1. Thermophysical Properties of AISI 1045 Carbon Steel[25]

Material	Density (kg/m^3)	Thermal conductivity (W/m·°C)		Specific heat capacity (J/kg·°C)	
AISI 1045 Carbon Steel	7870	212°F (100°C)	51.1	212°F (100°C)	486
		392°F (200°C)	49.0	392°F (200°C)	520
		752°F (400°C)	42.7	752°F (400°C)	599
		1112°F (600°C)	35.6	1112°F (600°C)	749

However, it was impossible to measure all temperatures inside the steel die using K-type thermocouples. Instead, temperatures for each depth of the steel are determined through interpolation and extrapolation plots with references to experimentally measured temperatures at seven different depths. Consequently, the heat flux of the steel die is calculated using Eqn. 4, considering the average temperature of the steel die for each time.

DESIGN OF EXPERIMENTS

MATERIALS

Two different steel die configurations were evaluated in this study. Cylindrical AISI 1045 carbon steel was used to fabricate the steel die having a composition of 0.43 to 0.5 wt.% C, 0.6 to 0.9 wt.% Mn, 0.04 wt.% P, 0.15 to 0.3 wt.% Si, 0.05% S, the balance being Fe. Thermal properties of the AISI 1045 steel are given in Table 1. Fig. 2 is a schematic of the two different configurations used in this study.

The die sample configuration shown in Fig. 2a was used for heating experiments with direct flame, as well as infrared heating. To record the thermal history the die was instrumented with K-type thermocouples, at different locations within the die to obtain a full thermal profile. The die sample configuration shown in Fig. 2b was employed for both heating and cooling experiments with cartridge heating, hot fluids, induction heating, and cooling water.

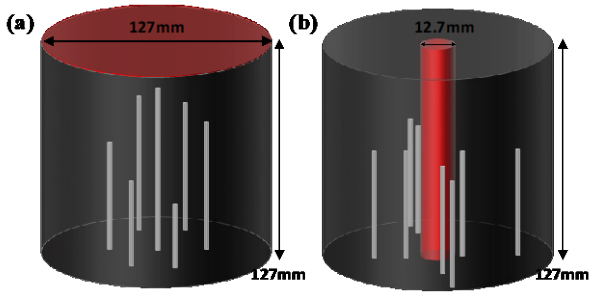

Figure 2. A schematic of two different steel die configurations used in this study. (a) for heating experiments with direct flame and infrared heating; (b) for both heating and cooling experiments with cartridge heating, hot fluids, and cooling water.

HEAT TRANSFER EXPERIMENTS

Heat transfer was quantitatively measured for various heating and cooling technologies; these included direct flame, hot fluids, cartridge heating, infrared heating, and jet water cooling. Thermal profiles were recorded for each thermal technology evaluated.

Accounting for heat losses

At the onset, it was necessary to establish the adiabatic conditions for the evaluation of thermal properties of the various thermal technologies considered. During heating of the steel die (Fig. 2), heat losses occur radially, which needed to be accounted for in the analyses. This was done by having the steel cylinder insulated with K-wool and ensured that uni-directional heat transfer conditions are applicable.

Specifically, heat losses were measured by having the steel cylinder heated to 842F(450C) for 1.5 hours in order to distribute heat uniformly throughout the sample in a Nabertherm NA250/45 furnace. Subsequently, the steel die was immediately inserted into a steel box completely encapsulated with K-wool insulation. Four thermocouples were inserted at different depths (3.3, 18.6, 32.7, and 63.5mm) throughout the steel and temperatures were recorded by a universal input touch screen data logger (OM-DAQXL-NA, OMEGA).

Direct Flame (Flame impingement)

As shown in Fig. 3, the steel die is exposed to the direct flame through an 18kg industrial propane tank. During the tests, mass flow rates with gas pressures were measured. Moreover, the effects of dimensionless separation distance (H/d) were also investigated ranging from 2 to 4. H refers to the distance between a torch and the surface of the steel die, and d is the diameter of a torch (73mm). Table 2 gives the experimental conditions.

Figure 3. Experimental direct flame setup.

Table 2. Experimental Variables for Gas Pressure, Mass Flow Rate & Dimensionless Separation Distance (H/d)

Gas pressure (psi)	Mass flow rate ($\times 10^{-4}$kg/s)	H/d
20	11.34	2
15	7.56	2
10	5.67	2
5	1.97	2
15	7.56	3
15	7.56	4

Temperatures were measured using several K-type thermocouples; one was located near the steel surface for the measurement of the flame temperature, and three others located inside the steel die at different depths. A boron-nitride paste was applied in each hole of the steel to minimize thermal resistance between the steel and the thermocouple.

Hot fluids (Hot oil and hot water)

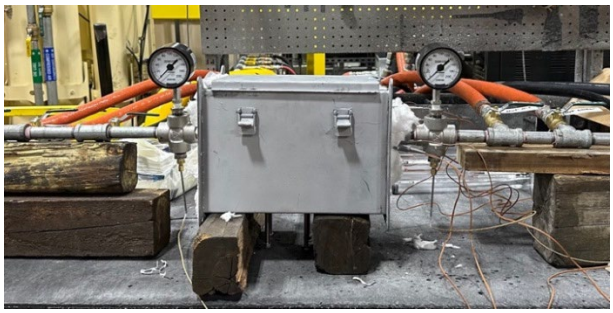

Figure 4. Experimental fluid setup for hot oil, hot water, and jet water.

Hot fluid experiments were conducted with hot oil and hot water at the Mercury Marine plant in Fond du Lac, Wisconsin. The steel die shown in Fig. 2b was used for these experiments. As shown in Fig. 4, 304 stainless steel pipes were connected to the central annulus of the steel cylinder allowing flow of the oil and water and fitted with pressure gauges and K-type thermocouples. Inlet and outlet pressures, as well as fluid temperature were monitored. The hot oil and hot water were managed by controllers (Regloplas-300LD/40/FM65/1K/RT100 and Regloplas-P160LD), respectively. The steel temperature was measured at different distances from the central channel of the steel.

Cartridge heating (Resistance heating)

Two cylindrical heating cartridges with an inserted thermocouple were prepared for two wattage conditions that were evaluated: 500 and 1000W. The steel sample shown in Fig. 2b was used and it was covered by K-wool insulation to prevent heat dissipation. Boron-nitride paste was applied at the cartridge/annulus interface to ensure heat transfer.

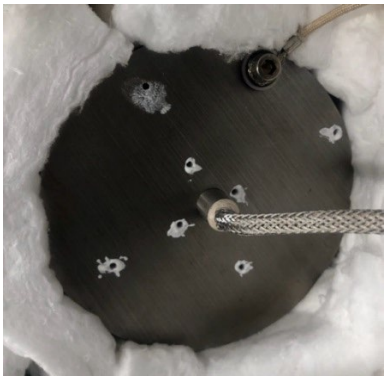

Figure 5. Image shows round cartridge heater inserted in the center of the steel sample.

The cartridge was inserted inside the steel sample, Fig. 5. A temperature controller (TSC-02) was employed in all the evaluations. Similar to previous heating trials, the steel was heated to 842F(450C). Temperatures inside the steel die were measured at different distances from the heating cartridge using K-type thermocouples and recorded with the data logger.

Infrared heating

Figure 6. Experimental infrared heating setup.

In infrared heating the mold coating material used in permanent molds influences has the potential to influence the emissivity and absorption of the infrared heater. Thus, one out of two samples had the surface coated with the mold coating used at ATEK Corp. to replicate conditions observed in industrial permanent molds. The steel die was heated to 550F(288C) before applying the coating. Three different coatings were used: (i) DAG-193 which is

an effective insulator and an excellent primer; (ii) CG-104 for controlling the texture and flow of the melt into the cavity; (iii) and PRODAG (Graphite) which is mainly used to release parts from the mold. The thickness of the coating layers was ~ 7mm.

Modular infrared heater OM1236.DV.3000 manufactured by INTEK Corp. was used in this work (Fig. 6). The infrared heater provided 4500W(3000W/ft^2) of energy with emitter surface dimensions of 305mm × 457mm. K-type thermocouples were used to measure the infrared emitter temperature as well as the temperature profile of the steel die sample. The steel surfaces were covered with K-wool insulation, except for one surface that was exposed to the infrared heater. During these heating tests, the effect of a coating and the distance between the infrared heater and the steel surface (12.7 and 50.8mm) on heat transfer were investigated.

Jet water cooling

Cooling trials with jet water coolers were performed using the same set up as shown in Fig. 4 and these tests were conducted at Mercury Marine Corporation. The experimental variables–flow rate, inlet pressure and outlet pressure used are given in Table 3. The jet water was managed by a Die Process Control System (Model 3.2.10 –19024R). The steel die temperature profile was obtained with the use of K-type thermocouples positioned at various depths in the die.

Table 3. Jet Water Cooling Variables–Flow Rate, Inlet Pressure & Outlet Pressure

Flow rate (ℓ/s)	Inlet pressure (psi)	Outlet pressure (psi)
0.271	22	20
0.397	42	40
0.497	62	60
0.606	92	90

MODELING AND SIMULATION WORKS

Heat transfer modeling and simulation were conducted to validate the heat transfer characteristics of various thermal technologies using Siemens Simcenter 3D software. The modeling and simulation utilized the same geometry model as the steel die used in the experiment. Thermo-physical properties of AISI 1045 tool steel, as shown in Table 1, were incorporated into the model. Although the density of the steel die varies with temperature, it was considered approximately constant due to the minor changes typically observed.[26] Subsequently, the inverse analysis method was employed to confirm the heat transfer values.[27] Heat transfer coefficients (h and IHTC) were used as boundary conditions to generate simulated temperatures influenced by various thermal technologies used in the experiments and assess the equivalence of experimental and simulated temperatures. Therefore, the experimentally measured steel die temperatures were used to validate the simulated temperatures of the model, along with the heat transfer values.

RESULTS AND DISCUSSION

h VALUE FROM HEAT LOSS EXPERIMENTS

Heat losses were measured by having the steel die which was heated to 842F(450C) and completely encapsulated with K-wool insulation cool down to 320F (160C); temperature was measured as a function of time, and the results are shown in Fig. 7. It took nearly 7 hours to have a 290°C (522°F) drop in temperature; a cooling rate of 0.009°C/s. K-wool insulation is a good thermal insulator as it should with such a low thermal conductivity (0.03W/m·°C).

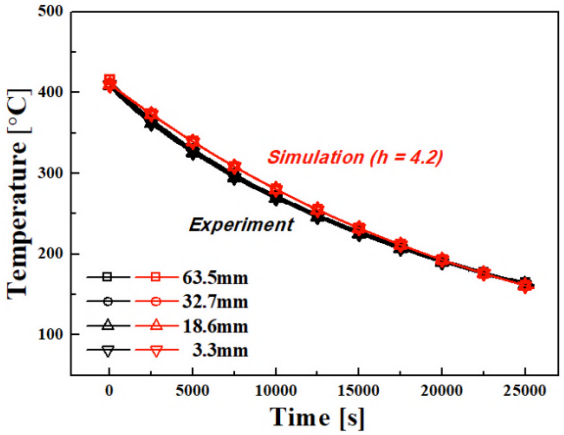

Figure 7. Temperature profile vs. time for the steel die during heat loss experiments.

To determine the uni-directional heat transfer condition for all thermal experiments, the convective heat transfer coefficient (h) of the insulation must be quantified and validated as the latter can be used for subsequent calculations and configurations. The inverse method was used with the experimental data shown in Fig. 7, and the h value of the insulation was verified to be 4.2W/m^2·°C. This value is applied in all subsequent calculations.

HEAT TRANSFER CHARACTERISTICS OF THERMAL TECHNOLOGIES

The results of the heating technologies that were investigated are given by reviewing the following: *(i)* effect of the processing variables on heating efficiency; *(ii)* The maximum temperature attained; *(iii)* the operative heat flux; and *(iv)* the effective heat transfer coefficient. For the cooling technology examined, similarly, operative heat flux and effective heat transfer coefficient are presented and discussed. This is followed by a discussion of the kinetics of heating and cooling of all five thermal management technologies investigated. Lastly, a discussion on efficient design of mold geometry is presented.

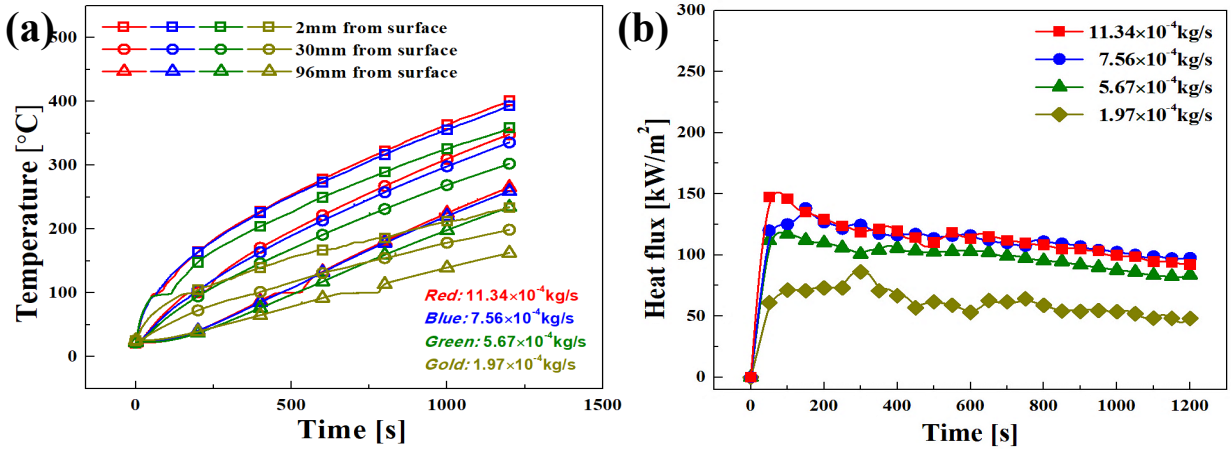

Figure 8. (a) Temperature and (b) heat flux vs time plot of the steel die influenced by direct flame with the variations of gas pressures.

Direct Flame (Flame impingement)

Direct flame primarily transfers heat through forced convection, and the highest heat flux from the flame is observed at the stagnation point within the reaction zone.[28] The stagnation regime extends over the impingement surface, spanning almost twice the burner diameter radially from the point of impingement.[29] In this experiment, axial effects were not considered as the stagnation regime encompassed the entire axial length of the steel die used. Therefore, the effects of mass flow rates and the ratio of H/d on heat transfer were examined.

As shown in Fig. 8a, the maximum temperatures of the steel die reached 574F(401C) at 11.34×10^{-4}kg/s and 739F(393C) at 7.56×10^{-4}kg/s by 1200 seconds, respectively. As the mass flow rate decreased, the maximum temperatures were 676F(358C) at 5.67×10^{4}kg/s and 451F(233°C) 451F at 1.97×10^{-4}kg/s. Moreover, the heat flux behavior of the steel die showed a similar trend to the temperature profiles, as shown in Fig. 8b. The highest average heat flux of the steel die indicated 153.5kW/m^2 at 11.34×10^{-4}kg/s, compared to 140.0kW/m^2 at 7.56×10^{-4}kg/s, 118.6kW/m^2 at 5.67×10^{-4}kg/s, and 86.5kW/m^2 at 1.97×10^{-4}kg/s, respectively. Following the temperature profiles and heat flux behaviors, higher mass flow rate with the high pressure resulted in higher temperature and heat flux of the steel attained, as the increased mass flow rates induced turbulent flow, enhancing heat transfer.

Additionally, in the context of flame impingement, the dimensionless separation distance (H/d) influences the shape of the flame. This ratio determines whether the inner reaction zone of the flame is intercepted by the surface of the steel die, thus affecting the heat flux and surface temperature of the steel die[8]. As exhibited in Fig. 9a, temperature distributions of the steel die were represented at different depths (2, 30, and 96mm) from the surface, corresponding to various H/d values (2, 3, and 4) with a constant mass flow rate of 7.56×10^{-4}kg/s.

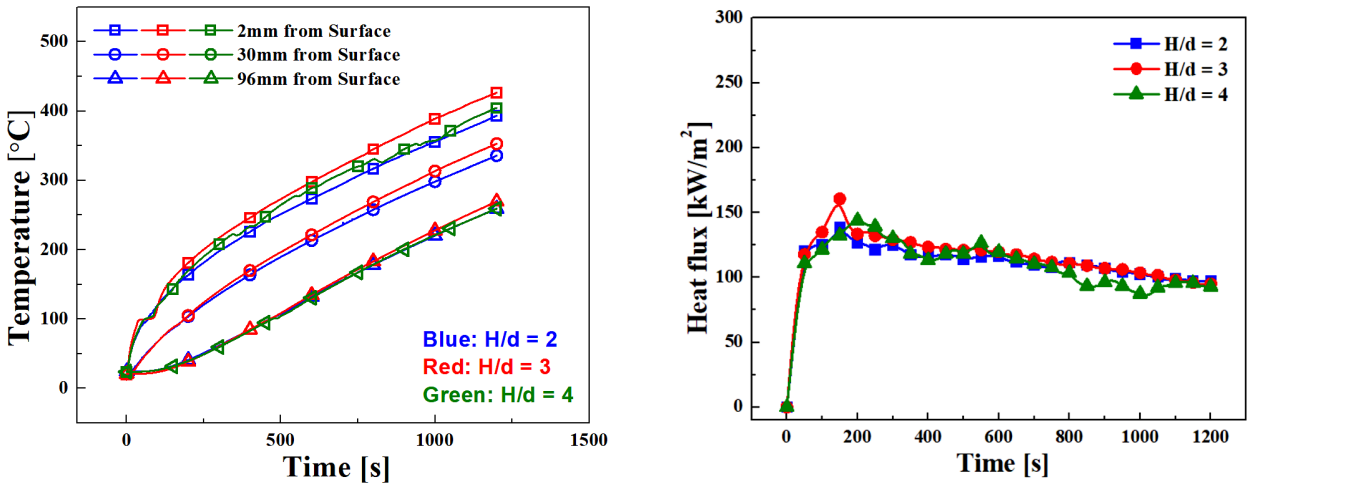

Figure 9. (a) Temperature vs. time; (b) heat flux vs. time plots of the steel die affected by direct flame with a variation of dimensionless separation distance (H/d).

Regarding the temperature profile, the surface temperature of the steel die showed fluctuation at the H/D ratio of 4. When the flame was impinged at a significant distance from the surface of the steel die, it was affected by the air in the atmosphere.

Unexpectedly, the temperature of the steel die did not reach its highest value when the flame torch was closest to the surface of the steel (H/d=2), showing 739F(393C) of its maximum up to 1200 seconds. Instead, the maximum temperature of the steel die indicated 800F(427C) at H/d=3 and 761F(405C) at H/d=4, respectively. Similarly, as seen in Fig. 9b, the average heat flux of the steel die showed the highest average value, 160.6kW/m^2, at H/D=3, compared to 140.0kW/m^2 at H/D=2 and 144.3kW/m^2 at H/D=4. It was deduced that the tip of the inner reaction zone made good contact with the impingement surface at H/D=3.[8] It results in both the highest surface temperature and heat flux. Conversely, the inner reaction zone was farther from the surface of the steel die when the H/d ratios were 2 and 4.

Convective heat transfer coefficients (h) of direct flame with various variables

Theoretically, heat conduction at the surface of the steel die is equal to the heat convection at the surface of the steel die in the same direction. The surface boundary cannot store energy, so the net heat entering the surface from the convective side must leave the surface from the conduction side.[30] Therefore, the h value is calculated with the obtained experimental data using Eqn. 2.

The inverse method was employed in modeling and simulation works to validate the h values of the direct flame under various mass flow rates and the ratio of H/d. As a result, the verified h values of the direct flame were indicated with various gas pressures in Fig. 10a; 81W/m^2·°C at 1.97×10^{-4}kg/s, 124W/m^2·°C at 5.67×10^{-4}kg/s, 133W/m^2·°C at 7.56×10^{-4}kg/s, and 134W/m^2·°C at 11.34×10^{-4}kg/s. Additionally, the effect of the H/d ratios on h value was represented, as shown in Fig.10b; 133W/m^2·°C at H/D=2, 163W/m^2·°C at H/D=3, and 140W/m^2·°C at H/D=4.

Hot fluids (Hot oil and hot water)

To investigate the effects of hot oil and water on heat transfer, temperature profiles of the steel die were measured at different distances (2, 30, and 96 mm) from the entrance of the hot fluids. The temperature behavior of the steel die is shown in Fig. 11a. For hot oil, the maximum temperature of the steel die reached 397F(203C) by 1800 seconds. However, the temperature approached 309F(154C) by 950 seconds during the hot water experiment. In addition, the temperature of the steel die showed limitations in further increase, irrespective of the fluids, due to the maximum fluid operating temperatures, which were recorded at 400F(204C) for hot oil and 320F(160C) for hot water.

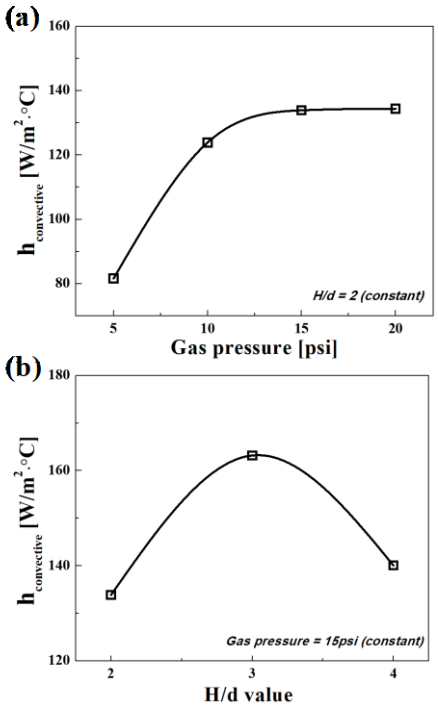

Figure 10. Convective heat transfer coefficients (h) of direct flame with variations of (a) gas pressure and (b) dimensionless separation distance (H/d).

Moreover, the average heat flux of the steel die was measured and is represented in Fig. 11b. For hot water, the average heat flux of the steel die initially indicated up to 201.9 kW/m^2 and then decreased gradually. Hot water increased its temperature rapidly from 82.4F (28C) to 212F (100C) in only 5 seconds. This rapid heating rate of hot water contributed to the initial high heat flux of the steel die. In contrast to hot water, hot oil reached its maximum heat flux slowly over 210 seconds, even though the initial temperature of hot oil (138F/59C) was higher than that of hot water (86F /30C). The highest heat flux of the steel die heated by hot oil was 137.4 kW/m^2, lesser than the hot water.

Convective heat transfer coefficients (h) of hot oil and hot water

Through the inverse method in modeling and simulation, it was confirmed that the simulated temperature profiles of the steel die were equivalent to the experimentally measured temperature profiles by applying the verified h values of hot oil and hot water, as shown in Fig. 12. Consequently, h values of hot water and hot oil were validated as 3580W/m^2·°C and 2050W/m^2·°C, respectively. The heat transfer to the steel was less effective with hot oil due to its lower thermal conductivity and higher viscosity than hot water. This was affirmed by the experimental heat transfer characteristics of both fluids.

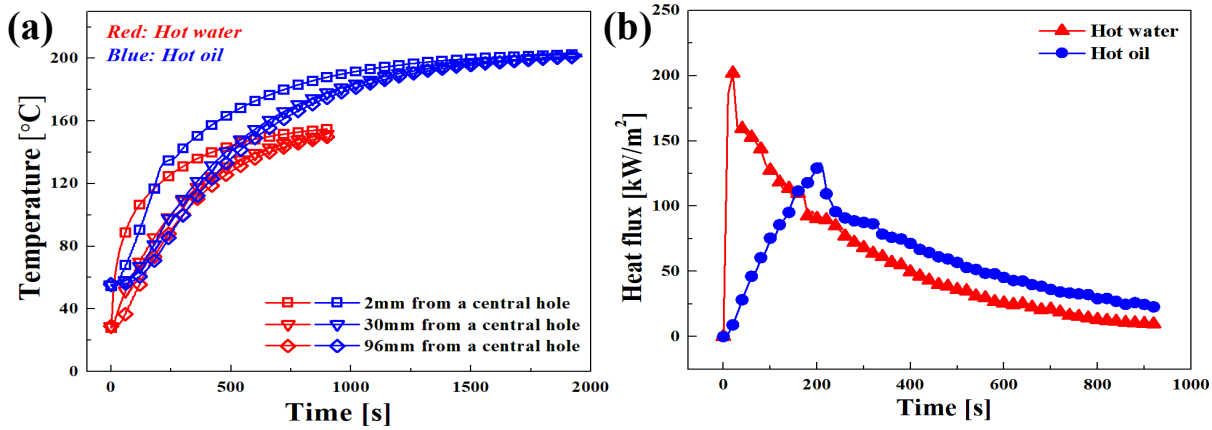

Figure 11. (a) Temperatures and (b) heat flux vs. time plots of the steel die affected by hot water and hot oil.

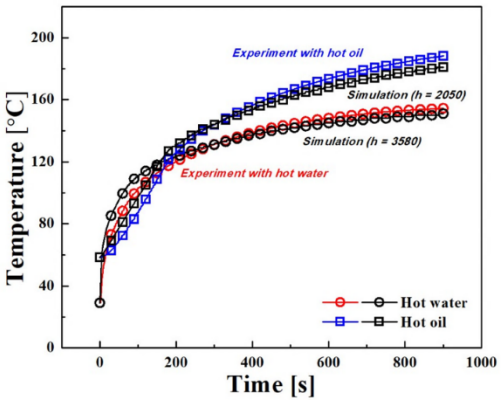

Figure 12. Experimentally measured and simulated temperature profiles vs. time plots measured near the entrance of hot fluids/annulus interface of the steel die heated by hot water and hot oil.

Cartridge heating (Resistance heating)
Effects of heating cartridge powers (500W and 1000W) on heat transfer

The cartridge heating experiments investigated the effects of heating cartridge powers (500W and 1000W) on heat transfer. Temperature profiles of the steel die heated by the heating cartridge were measured at different distances (2, 25, and 55mm) from the cartridge/annulus interface, as shown in Fig. 13. In the temperature profiles of the heating rods, the 1000W heating rod reached a maximum temperature of 842F(450C) in 1760 seconds. However, the 500W heating rod took 4590 seconds to reach the same maximum temperature of 842F(450C). Despite initial heating rates of 3.3°C/s at 1000W and 2.9°C/s at 500W, these rates significantly decreased to 0.13°C/s and 0.07°C/s, respectively.

For temperature profiles of the steel dies, the temperatures reached 790F(421C) and 750F(399C) as their maximum temperatures at 3600 and 4640 seconds for 1000W and 500W heating power, respectively, as shown in Fig. 13. Unlike other heating technologies previously, the temperature of the steel die increased slowly with 0.16 and 0.09°C/s of average heating rates at both heating

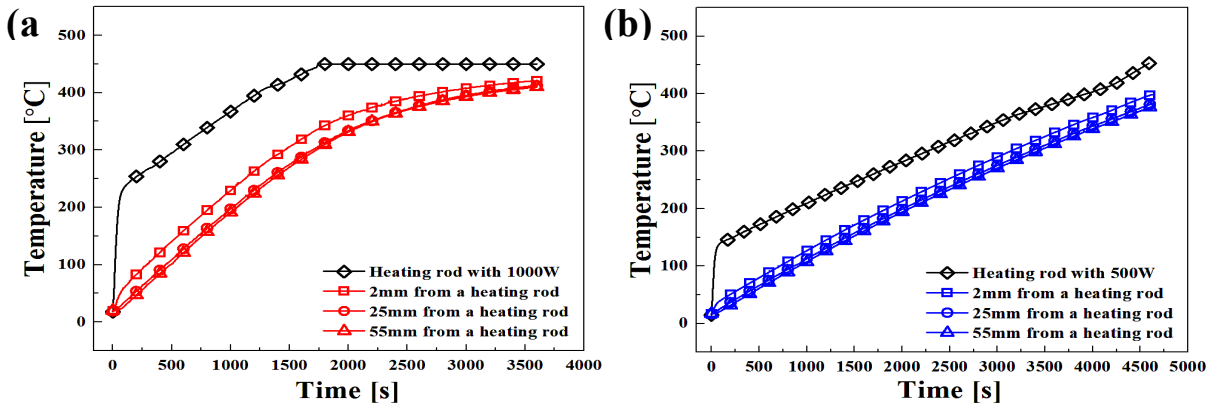

Figure 13. Temperature vs. time plots of heating cartridges and the steel die affected by (a) 1000W and (b) 500W of heating cartridges.

powers. The slow heating rate of the steel die was followed by the heating rate of the heating rod, as discussed previously. In addition, heat fluxes near the interface of the steel die were exhibited in Fig. 14. With a rapid temperature increase in the heating rod, initial average heat fluxes by 1000W and 500W of heating cartridges reached 90.7kW/m^2 and 47.6kW/m^2 at maximum. However, they decreased gradually over time, see Fig. 14.

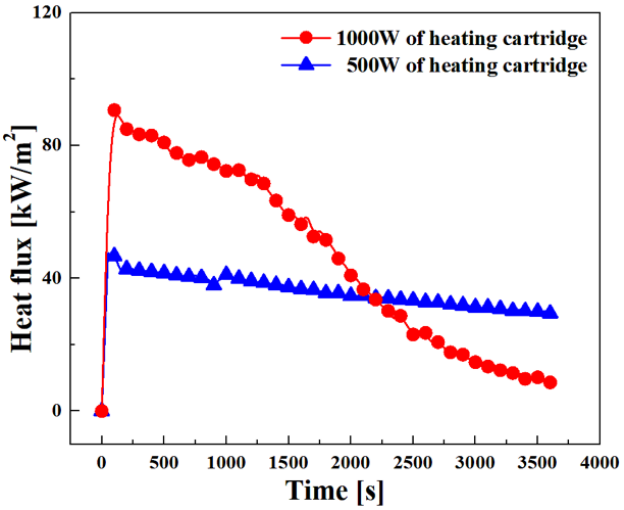

Figure 14. Average heat flux vs. time plots of the steel die heated by 1000W and 500W of heating cartridges.

Interfacial heat transfer coefficient (IHTC) at the interface between the steel die and the heating cartridge

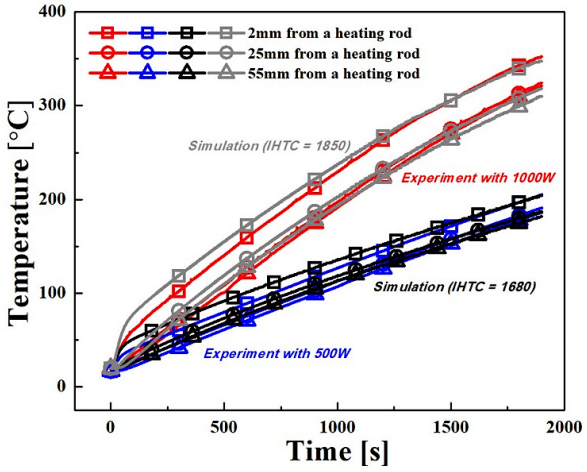

Figure 15. Experimentally measured and simulated temperature profiles vs. time plots measured near the cartridge/annulus interface of the steel die heated by 1000W and 500W of heating cartridges.

Unlike direct flame and hot fluid heating technologies, there were no convection heat transfer effects by a heating cartridge in this test. Instead, heat transfer occurs mainly by the conduction heat transfer from a heating cartridge. The IHTC value is identified quantitatively with the experimental data, following Eqn.4.[24] Based on the inverse method in modeling and simulation, it was confirmed that the experimentally measured temperature profile of the steel die was well matched with the simulated temperature profile when the IHTC values were applied as both 1850W/m^2·°C at 1000W and 1680W/m^2·°C at 500W in Fig. 15.

Infrared heating

Radiation heat transfer occurs mainly from the emission and absorption of electromagnetic waves. In this test, the infrared heater emits thermal energy as a form of infrared radiation, and it is subsequently absorbed by the surface of the steel dies. The temperature profile of the steel die was measured at different depths (2, 30, and 96mm) from the outer surface. Prior to investigating the effect of distance from the infrared heater on heat transfer, we examined the effect of a coating on the outer surface of the steel die at a constant distance from the heater (12.7mm), as shown in Fig. 16.

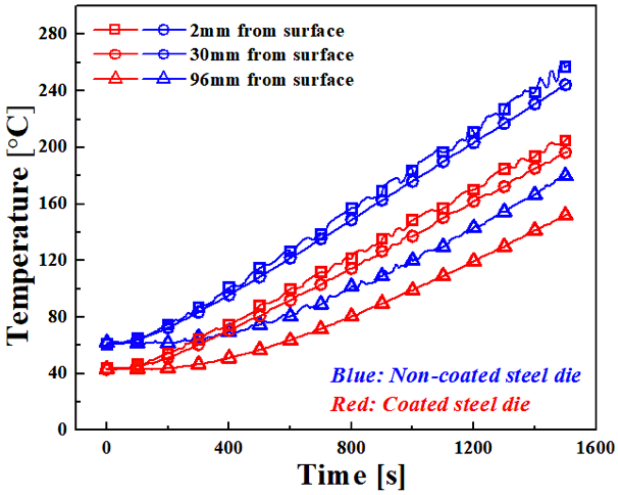

Figure 16. Temperature vs. time plots of the non-coated and coated steel die affected by an infrared heater with a constant distance from the heater (12.7mm).

The temperature of the non-coated steel die reached a maximum of 496F (258C). In contrast, that of the coated steel die was 401F (205C), even though the initial temperatures of the steel die were different. However, we observed minimal the effect of a coating on heat transfer. Moreover, the average heating rate of the non-coated steel die was 0.14°C/s, similar to the 0.12°C/s observed for the coated steel die.

Additionally, the effects of the distance between the infrared heater and the steel die were investigated, as seen in Fig. 17.

The temperature of the steel dies increased to 401F (205C) and 266F(130C) at their maximum at distances of 12.7 and 50.8mm from the infrared heater until 1500 seconds, respectively.

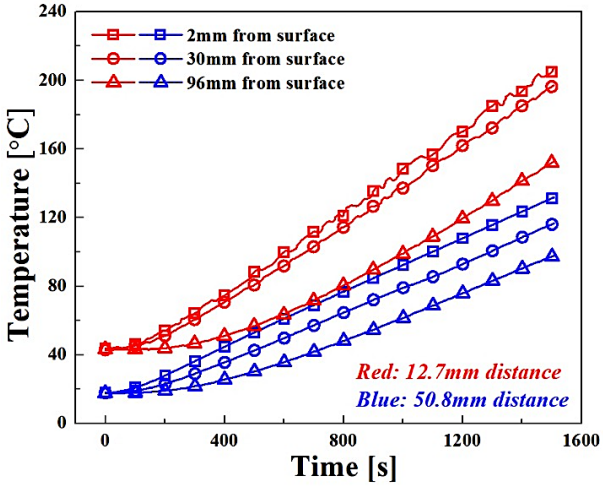

Figure 17. Temperature vs. time plots of the coated steel dies affected by an infrared heater with variations of a distance from the heater.

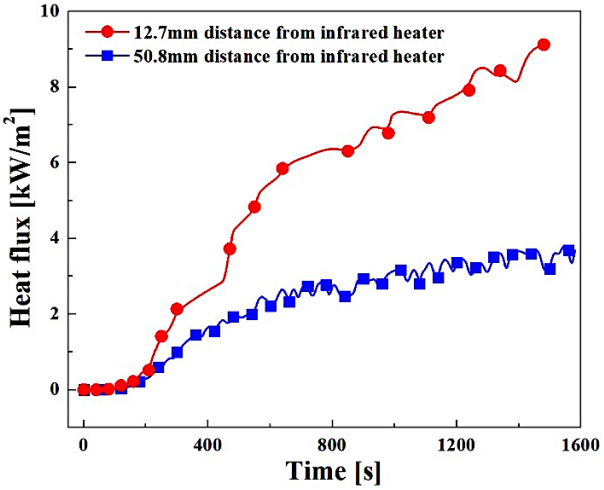

Figure 18. Heat flux vs. time plots of the coated steel dies affected by an infrared heater with variations of a distance from the heater.

Although the initial temperatures of the steel dies differed under each distance, the temperature increase was more rapid at the closer distance (12.7mm) than at the farther distance (50.8mm) from the infrared heater. The result was evident from the fact that the average heating rate of the steel die was 0.12°C/s at the closer distance, whereas it was 0.08°C/s at the farther distance. By using the experimentally measured temperatures of the steel die, the heat flux of the steel die by radiation is calculated, following Eqn.6.

$$q = \varepsilon \cdot \sigma \cdot (T_s^4 - T_\infty^4) \qquad \text{Eqn.6}$$

Where: q = heat flux (W/m^2), ε = emissivity of the surface on the steel, σ = Stefan-Boltzmann constant, and T_s and T_∞ = temperatures of a radiating surface on the steel and infrared heater (°C), respectively.

Figure 18 showed heat fluxes measured near the surface over time. Irrespective of distances from the heater, the heat flux gradually increased as a function of time. Like the temperature profile, the heat flux was higher at the closer distance (12.7mm) than the farther distance (50.8mm) from the heater. This decrease in intensity followed the inverse square law,[31] which states that the radiation intensity diminishes significantly as the distance from the heater squared increases. Consequently, less thermal energy was transferred to the steel die farther from the heater. In addition, thermal energy may have been lost as it interacted with the medium between the heater and the steel die, such as air. Through the validation in modeling and simulation, average heat fluxes were determined as 3.85kW/m² at 12.7mm and 2.33kW/m² at 50.8mm from the infrared heater, respectively.

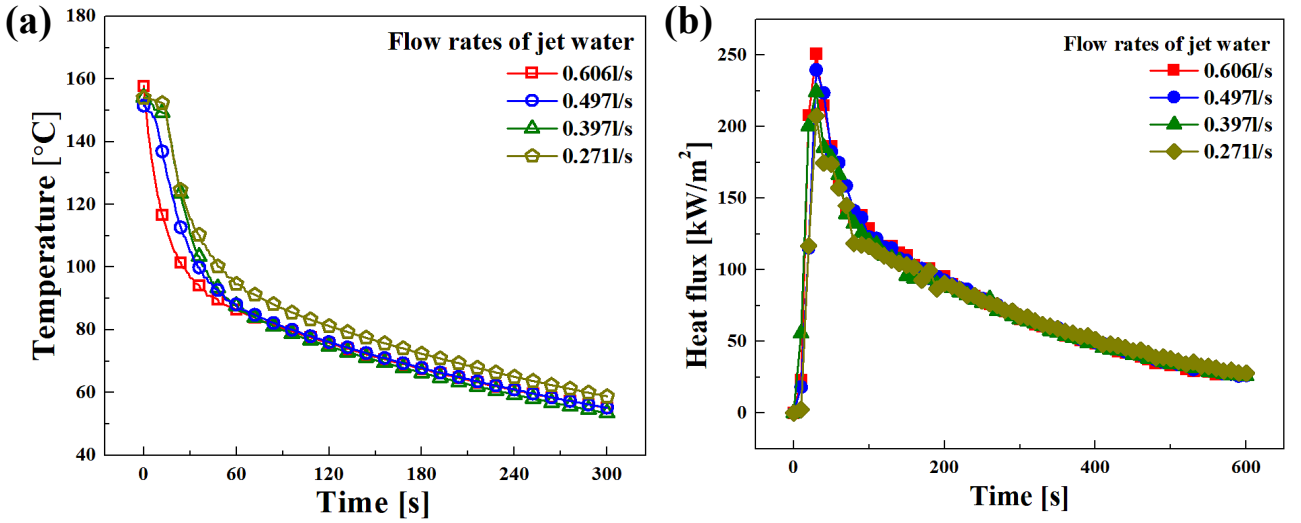

Figure 19. (a) Temperature vs. time and (b) average heat flux vs. time plots of the heated steel die cooled by jet water with various flow rates.

Jet water cooling

Jet water cooling trials were conducted using various flow rates of jet water immediately after the hot fluid tests. The objective of these experiments was to investigate the effect of jet water flow rates on heat transfer. For this purpose, temperature profiles of the steel die were measured at 2mm from the entrance of the jet water.

As shown in Fig. 19a, jet water exhibited efficient thermal performance, enabling rapid heat dissipation from the heated steel die. Remarkably, under the fastest jet water flow rate (0.606ℓ/s), the temperature of the steel die decreased rapidly to below 212F (100C) within 30 seconds, representing a cooling rate of 2.5°C/s. Cooling rates at other flow rates were relatively slower: 2.3°C/s at 0.497ℓ/s, 2.0°C/s at 0.397ℓ/s, and 1.6°C/s at 0.271ℓ/s. Higher flow rates of jet water increased turbulence by effectively mixing the fluids, resulting in rapid cooling of the steel die. In addition, average heat fluxes of the steel dies are represented in Fig. 19b. The maximum average heat flux of the steel die was observed showed at 0.606 ℓ/s (251.1kW/m²), followed by 0.497ℓ/s (239.7kW/m²), 0.397ℓ/s (224.3kW/m²), and 0.271ℓ/s (207.4kW/m²), respectively.

Convective heat transfer coefficients (h) of the jet water with a variation of flow rates

The inverse method was employed in modeling and simulation to validate the h values of the jet water. As a result, the validated h values of the jet water are presented in Fig. 20 for various flow rates: 2220W/m²·°C at 0.271ℓ/s, 2820W/m²·°C at 0.397ℓ/s, 3330W/m²·°C at 0.497ℓ/s, 3600W/m²·°C at 0.606ℓ/s.

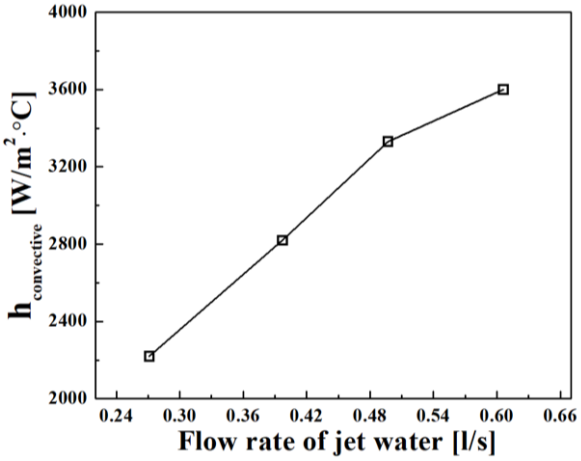

Figure 20. Convective heat transfer coefficients (h) of jet water with a variation of flow rates.

Kinetics of heating and cooling technologies on the same geometry by modeling and simulation works.

Heat transfer characteristics of various thermal technologies were investigated through modeling and experimental work. However, comparing the kinetics of heating and cooling under the same conditions was challenging because the experimental tests used two different steel die configurations and varying initial temperatures of the steel dies. To enable a comparison of kinetics for thermal technologies under identical conditions, a simple cubic model (254 mm × 254 mm × 254 mm) was used in modeling and simulation. Applying the thermo-physical properties of AISI 1045 carbon steel, as shown in Table 1, into the model, the kinetics and temperature behaviors of the steel die model using various thermal technologies were investigated. In this work, all temperatures of heating technologies were set as their maximum operating temperatures. Furthermore, it was assumed that all surfaces are covered with K-wool insulation by applying the validated h value of insulation as same as the experimental condition, except for the outer surface.

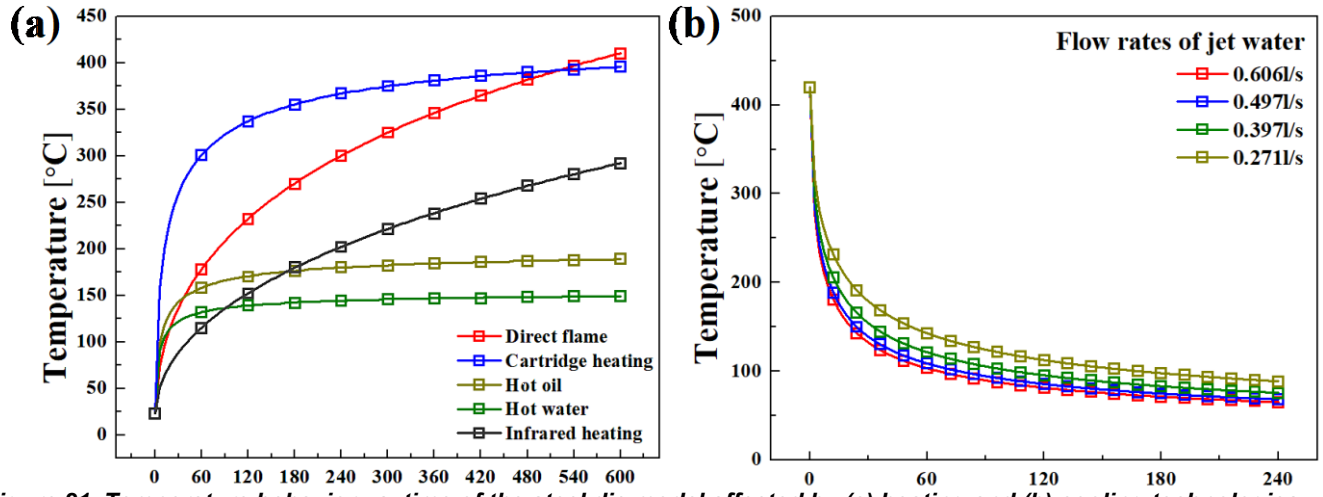

Figure 21. Temperature behavior vs. time of the steel die model affected by (a) heating and (b) cooling technologies in simulation works.

The validated h and IHTC values for direct flame, hot oil, hot water, jet cooling water, and cartridge heating were applied. Moreover, the verified heat flux by infrared heating was also employed.

In Fig. 21, the temperature of the steel die model on the surface was obtained during heating and cooling. For heating technologies in Fig. 21a, the highest temperature of the steel die model was noted at 770F (410C) at 600 seconds by direct flame. The maximum steel temperatures recorded for other technologies were 745F (396C) by cartridge heating, 558F (292C) by infrared heating, 372F (189C) by hot oil, and 300F (149C) by hot water. As discussed earlier, both hot fluids showed a limitation in increasing the steel die temperature due to their maximum operating temperature.

To efficiently compare the kinetics of heating technologies, we needed to consider the adequate heating time for permanent mold casting, as it significantly impacts the casting production time. Therefore, an efficient heating time of 90 seconds was selected. According to this critical heating time, the heating rates of the steel die model were 3.38°C/s by cartridge heating, 2.06°C/s by direct flame, 1.59°C/s by hot oil, 1.26°C/s by hot water, and infrared heating at 1.26°C/s. Consequently, cartridge heating represented the highest kinetic performance among these heating technologies. These findings open up the possibility of efficiently utilizing certain heating technologies for both the heating cycle and pre-heating applications in permanent molds.

For the cooling simulation, as depicted in Fig. 21b, the initial temperature of the steel die model was set at 788F (420C). Similar to heating technologies, an efficient cooling time of 60 seconds was chosen, considering the necessity for rapid heat dissipation in a dynamic casting system. The kinetics were observed as follows: the highest water flow rate (0.606ℓ/s) exhibited the highest kinetic performance at 8.72°C/s, followed by 8.53°C/s at 0.497ℓ/s, 8.09°C/s at 0.397ℓ/s, and 7.36°C/s at 0.271ℓ/s. These results aligned with our cooling experimental findings.

CONCLUSIONS

This paper aims to evaluate the heat transfer characteristics of various thermal technologies both experimentally and through modeling and simulation. The goal is to identify efficient applications for local thermal management in the permanent mold casting system. Therefore, quantitative heat transfer values of heating and cooling technologies were provided under several operating conditions: (i) the maximum temperature that can be attained by the steel die, (ii) the heat flux, (iii) convective (h) and interfacial heat transfer coefficients (IHTC), and (iv) the kinetics of heating/cooling technologies. The main conclusions of this study can be summarized as follows:

1. Heat loss characteristics with insulation were initially examined to establish adiabatic conditions for all thermal technology experiments. The K-wool insulation showed excellent thermal insulating properties with a cooling rate of 0.009°C. Through experiments and modeling work, the h value of the K-wool was validated as 4.2W/m^2·°C and was subsequently applied in all heating and cooling modeling and simulation studies.

2. The heat transfer behaviors of direct flame were investigated, considering variations in mass flow rates and the dimensionless separation distance (H/d). For the mass flow rates (1.97×10^{-4}, 5.67×10^{-4}, 7.56×10^{-4}, and 11.34×10^{-4} kg/s), the highest average heat flux and maximum temperature of the steel die were 153.5kW/m^2 and 574F(401C) at a mass flow rate of11.34×10^{-4}kg/s, respectively. Interestingly, both heat transfer values were slightly lower at a mass flow rate of 7.56×10^{-4}kg/s, showing 140.0 kW/m^2 for the average highest heat flux and 676F(358C) as the maximum temperature. The h values were also validated as 81, 124, 133, and 134W/m^2·°C, corresponding to each mass flow rate variable. Additionally, Moreover, a peak average heat flux of 160.6kW/m^2 on the steel die was observed when the H/d ratio was 3, while it showed 140.0kW/m^2 at H/D=2 and 144.3kW/m^2 at H/D=4. It is assumed that the flame tip of the inner reaction zone was in close contact with the surface at H/D=3. The h values represented 133, 163, and 140W/m^2·°C, depending on H/d values. Considering gas consumption and heat transfer behaviors, it would be worthwhile to explore the application of direct flame with a mass flow rate of 7.56×10^{-4} and the H/d ratio of 3.

3. The effects of hot water and hot oil on heat transfer were examined. The average highest heat flux of the steel die heated by hot water was 201.9kW/m^2, higher than the 137.4kW/m^2 achieved with hot oil. In addition, the h values for hot water and hot oil were determined to be 3580 and 2050 W/m^2·°C, respectively. This was attributed to the lower thermal conductivity and higher viscosity of hot oil than hot water, resulting in reduced heat transfer capability of hot oil to the steel.

4. The effects of heating cartridge powers (500W and 1000W) on heat transfer were investigated. The steel die reached 790°F(421°C) with 1000W and 750°F(399°C) with 500W as the maximum temperatures at 3600 and 4640 seconds, respectively. Furthermore, the average heat flux of the steel die with 1000W (90.7kW/m^2) was higher than that with 500W (47.6kW/m^2). As expected, in line with heat

flux behaviors, the interfacial heat transfer coefficient (IHTC) value of the steel die heated by the 1000W heating cartridge indicated 1850W/m^{2}·°C, which is larger than the 1680W/m^{2}·°C with the 500W heating cartridge.

5. The heat transfer behaviors of infrared heating were studied with variations in the distance from the infrared heater (12.7 and 50.8mm), as well as the effects of coating on heat transfer. Although the initial temperatures of the coated and non-coated steel dies differed, few changes were observed. This was evident in the heating rates, where the non-coated steel die exhibited a rate of 0.14°C/s, while the coated steel die indicated 0.12°C/s. In terms of the variation in distance, the temperatures of the coated steel dies increased to 401F(205C) and 266F(130C) at 12.7 and 50.8mm from the heater, respectively, until 1500 seconds. It was found that the average heating rate of the coated steel die was 0.12°C/s at the closer distance (12.7mm) and 0.08°C/s at the farther distance (50.8mm). Additionally, the average heat fluxes at 12.7mm and 50.8mm from the infrared heater were determined to be 3.85kW/m² and 2.33kW/m², respectively.

6. In the cooling trials, the highest flow rate (0.606 ℓ/s) of jet water exhibited the highest cooling rate of 2.5°C/s and the highest average heat flux of 251.1kW/m². Additionally, as the flow rate of the jet water decreased, both heat flux and cooling rate decreased. This is because high flow rates increase turbulence by mixing fluids effectively, resulting in rapid heat dissipation. Furthermore, the h values of the jet water were verified as 2220, 2820, 3330, and 3600 W/m²·°C at each flow rate, respectively, through experiments and modeling.

7. The kinetics of all evaluated thermal technologies were compared using the same geometry in the modeling and simulation works. In this study, validated h and IHTC values, as well as heat flux values from infrared heating, were applied. Among the heating technologies, the heating rates of the steel die model were 3.38°C/s for cartridge heating, 2.06°C/s for direct flame, 1.59°C/s for hot oil, and 1.26°C/s for both hot water and infrared heating. It can be assumed that the cartridge heater can rapidly increase the temperature of the steel die, particularly when the heating rod operates at its maximum temperature, among all evaluated heating technologies. In terms of jet water cooling, consistent with the experimental results, the highest kinetic performance was achieved at the highest water flow rate (0.606 ℓ/s), registering 8.72°C/s. This was followed by 8.53°C/s at 0.497 ℓ/s, 8.09°C/s at 0.397 ℓ/s, and 7.36°C/s at 0.271 ℓ/s.

ACKNOWLEDGMENTS

The authors wish to acknowledge the Advanced Casting Research Center for supporting this research. The authors wants to thank Adam Kopper at Mercury Marine for help, Addam Drewelow at ATEK Corp. for help with mold coatings, and Jesse Stricker and Ruben Aramburu at INTEK Corp. for help with infrared experiments.

REFERENCES

1. Sirinterlikci, A., "Thermal management and prediction of heat checking in H-13 die-casting dies," The Ohio State University (2000).
2. Campbell, J., "Complete casting handbook: metal casting processes, metallurgy, techniques and design," Butterworth-Heinemann (2015).
3. Wang, H., Yu, W. & Cai, Q., "Experimental study of heat transfer coefficient on hot steel plate during water jet impingement cooling," *Journal of Materials Processing Technology,* 212, 1825-1831 (2012).
4. Choi, J. W. & Choi, J. W., "Convective heat transfer coefficient for high pressure water jet," *ISIJ international,* 42, 283-289 (2002).
5. Liu, Z.-H., Tong, T.-F., & Qiu, Y.-H., "Critical heat flux of steady boiling for subcooled water jet impingement on the flat stagnation zone," *J. Heat Transfer,* 126, 179-183 (2004).
6. Lee, P., Choi, H. & Lee, S., "The effect of nozzle height on cooling heat transfer from a hot steel plate by an impinging liquid jet," *ISIJ international,* 44, 704-709 (2004).
7. Oppelt, T., Schulze, J., Stein, H. & Platzer, B., "Comparison of methods for mould surface heating–Part 1," *International Polymer Science and Technology* 39, 1-8 (2012).
8. Chander, S. & Ray, A., "Heat transfer characteristics of laminar methane/air flame impinging normal to a cylindrical surface," *Experimental Thermal and Fluid Science,* 32, 707-721 (2007).
9. Virk, A. S., "*Heat transfer characterization in jet flames impinging on flat plates*," Virginia Tech, (2015).
10. Kozanoglu, B., Zárate, L., Gómez-Mares, M. & Casal, J., "Convective heat transfer around vertical jet fires: An experimental study," *Journal of hazardous materials,* 197, 104-108 (2011).
11. Jeng, M.-C., Chen, S.-C., Minh, P. S., Chang, J.-A. & Chung, C.-s., "Rapid mold temperature control in injection molding by using steam heating," *International Communications in Heat and Mass Transfer,* 37, 1295-1304 (2010)
12. Ferraro, V., Settino, J., Cucumo, M. & Kaliakatsos, D., "Parabolic trough system operating with nanofluids: comparison with the conventional working fluids and influence on the system

performance," *Energy procedia,* 101, 782-789 (2016).
13. Chang, P.-C. & Hwang, S.-J., "Simulation of infrared rapid surface heating for injection molding," *International Journal of Heat and Mass Transfer,"* 49, 3846-3854 (2006).
14. Wang, W. *et al.,* "Radiative heat transfer behavior of mold fluxes for casting low and medium carbon steels," *ISIJ international,* 51, 1838-1845 (2011).
15. Hu, H., Chen, F., Chen, X., Chu, Y.-l. & Cheng, P., "Effect of cooling water flow rates on local temperatures and heat transfer of casting dies," *Journal of Materials Processing Technology* 148, 57-67 (2004).
16. Schubotz, S. & Nacke, B., "Modelling and verification of convective heat transfer coefficient for induction applications," *International Journal of Applied Electromagnetics and Mechanics,* 53, S79-S88 (2017).
17. Venkatesh, G. & Kumar, Y.R., "Thermal analysis for conformal cooling channel," *Materials Today: Proceedings,* 4, 2592-2598 (2017).
18. Flemings, M.C., "Solidification processing," *Metallurgical and Materials Transactions B,* 5, 2121-2134 (1974).
19. Lavernia, E.J. & Srivatsan, T.S., "The rapid solidification processing of materials: science, principles, technology, advances, and applications," *Journal of Materials Science,* 45, 287-325 (2010).
20. Stefanescu, D., Davis, J. & Destefani, J., "Metals Handbook, Vol. 15-Casting," *ASM International,* 937 (1988).
21. Roorda, S., "Influence of Mold Coating Wear on Heat Transfer Coefficient in Aluminum Permanent Molds," Worcester Polytechnic Institute (2021).
22. Stefanescu, D.M. & Stefanescu, D.M., "Solidification of metal matrix composites," *Science and Engineering of Casting Solidification*, 305-341 (2015).
23. Winterton, R., "Newton's law of cooling," *Contemporary Physics,* 40, 205-212 (1999).
24. Dhodare, A., Ravanan, P. & Dodiya, N., "A review on interfacial heat transfer coefficient during solidification in casting," *IJERT,* 6, 464-467 (2017).
25. Brandes, E.A. & Brook, G., "Smithells metals reference book," Elsevier (2013).
26. Hung, T.-P., Shi, H.-E. & Kuang, J.-H., "Temperature modeling of AISI 1045 steel during surface hardening processes," *Materials,* 11, 1815 (2018).
27. Beck, J.V., "Surface heat flux determination using an integral method," *Nuclear Engineering and Design,* 7, 170-178 (1968).
28. Zhen, H. *et al.,* "An experimental examination of the role of turbulence on flame impingement heat transfer," *Fuel,* 268, 117329 (2020).
29. Kuntikana, P. & Prabhu, S, "Impinging premixed methane-air flame jet of tube burner: thermal performance analysis for varied equivalence ratios," *Heat Mass Transfer,* 55, 1301-1315 (2019).
30. Incropera, F.P., DeWitt, D.P., Bergman, T.L. & Lavine, A.S., "Fundamentals of heat and mass transfer," Vol. 6, Wiley, New York (1996).
31. Voudoukis, N. & Oikonomidis, S., "Inverse square law for light and radiation: A unifying educational approach," *European Journal of Engineering and Technology Research,* 2, 23-27 (2017).